Induction Heating of Aluminum Billets Subjected to a Strong Rotating Magnetic Field Produced by Superconducting Windings

Thierry Lubin, Denis Netter, Jean Lévêque, Abderrezak Rezzoug

Induction Heating of Aluminum Billets Subjected to a Strong Rotating Magnetic Field produced by Superconducting Windings

Thierry Lubin, Denis Netter, Jean Leveque and Abderrezak Rezzoug

Groupe de Recherche en Electrotechnique et Electronique de Nancy, GREEN, CNRS UMR 7037, FRANCE

This paper presents an analysis of an original structure of induction heater using superconducting coils. With the proposed structure, two operating modes are possible to heat the aluminum billet. Either the billet is at standstill and placed within a strong rotating magnetic field (around 3.5 T) of low frequency (around 1 Hz), or the billet rotates at low angular speed (around 6 rad/s) within a strong DC magnetic field (around 3.5 T). The analysis is based on the analytical solution of two-dimensional diffusion equations for the magnetic vector potential. A closed-form expression is derived for the eddy-current power loss in the billet. This analytical expression can be used as a tool for design optimization of the induction heater. The analytical results are compared with those obtained with Finite Element Method (FEM) software. The study of the temperature field in the billet shows that a homogeneous temperature profile is obtained when a strong magnetic field of low frequency (rotating speed or AC current pulsation) is used.

***Index Terms*— Analytical solution, eddy-current, induction heater, superconducting coils, temperature.**

I. Introduction

Induction heating is used in industrial processes for any applications where it is needed to heat an electrical conductive material in an efficient and controlled manner. A particular application concerns the press-forming process of aluminum billets. The billet is pre-heated at a temperature of about 500 °C before it is placed into the forming press. It is important to reach a temperature distribution as uniform as possible in the billet for the quality of the forming process [1]. In conventional induction heater, the aluminum billet is axially placed within a water cooled copper coil supplied by an alternating current with a frequency of 50 Hz. The efficiency of this type of induction heater for a rated power of about 1 MW is only around 50%.

In order to improve the efficiency, Runde and Magnusson [2]-[4] have studied and designed a new type of induction heater (10 kW) by replacing the conventional copper coil by high-temperature superconducting (HTS) coil excited with 50/60 Hz alternating current. However, because of the AC losses in HTS coil, the efficiency obtained with the small-scale demonstrator does not exceed 60%. More recently, in the setting of a European project called ALUHEAT, a new induction heater design (200 kW) with superconducting coils has been proposed [5],[6]. The aluminum billet rotates at 3000 rpm in a static magnetic field generated by superconducting coil fed by DC current. The rotation causes the circulation of induced current in the billet and produces heat by the Joule effect. The billet is driven by an electrical machine and the efficiency can reach 90% which is the efficiency of an electrical motor. The analysis of eddy-current power losses distribution in the rotating billet has been studied in [5] by using simple electrical circuit method or FEM software. The cryogenic design of the ALUHEAT project is developed in [7]. The temperature distribution in aluminum billets heated by rotation in static magnetic field has been studied by [8]. A numerical model, based on an equivalent electric network has been developed. Results obtained for an aluminum billet rotating at angular velocities of 3000 rpm and 1500 rpm in a static magnetic field of 0.5 T have shown a strong temperature gradient in the radial direction.

In this paper, we propose an analysis of an original structure for induction heating of aluminum billet using superconducting coils. This structure allows to obtain a homogeneous temperature profile in the billet. The description of the studied induction heater is given in section II. An analytical model is then developed in sections III and IV for determining the eddy current density and power loss density in the aluminum billet. Simplified expressions for large skin depth are then provided. Finally, the temperature profile in the billet is obtained with two-dimensional finite element method software (COMSOL).

II. Description of the Induction Heater

Fig. 1 and Fig. 2 show respectively the cross section of the 2 poles and 4 poles configuration for the induction heater studied in this paper. The induction heater consists of two phase superconducting windings (the windings are named A and B) placed at right angle to each other around the cryostat. The winding schemes for two poles and four poles configuration are given in Fig. 3 and Fig. 4. The aluminum billet to be heated is placed inside the warm hole of the cryostat. The main parameters of the induction heater are given in Table I. The geometrical parameters have been chosen arbitrarily in order to verify the analytical model developed in the paper.

Two operating modes are possible to heat the billet. In the first one, the billet is at standstill and is subject to a strong rotating magnetic field (around 3.5 T) of low frequency

Digital Object Identifier inserted by IEEE

(around 1 Hz) which induces current in it. To obtain a rotating magnetic field, the superconducting windings must be fed by alternating currents with a phase shifted by 90 degrees. The rotating magnetic field rotates at an angular velocity related to the electrical current frequency ω and the number of pole pairs of the winding configuration. In the second operating mode, the aluminum billet rotates at low angular speed (around 6 rad/s) within a strong DC magnetic field (around 3.5 T). The rotation of the billet causes the circulation of induced currents which produce Joule heating in it. To generate a static magnetic field, only one superconducting winding (winding A or winding B) has to be fed by a DC current. The use of low frequencies for the rotating magnetic field or for the billet angular speed allows obtaining a large skin depth and therefore a homogeneous temperature in the billet. In a physical viewpoint, these two operating modes are equivalent for the same field amplitude and taking approximately the first space harmonics of the current distribution. It will be shown further in the paper that the equations governing the induced current are the same in the two cases.

TABLE I
INDUCTION HEATER PARAMETERS USED FOR ANALYSIS

Symbol	Quantity	Value
R_1	Aluminum billet radius	8 cm
R_2	Superconducting winding inner radius	13 cm
e	Superconducting winding thickness	4 cm
α	Span angle of the winding	$\pi/10$ rad
β	Winding slot pitch	$\pi/8$ rad
L	Billet axial length	1 m
Ω	Angular speed of the billet	variable
ω	Electric current pulsation	variable
σ	Electrical conductivity of the billet (aluminum)	$37.10^6\ \Omega^{-1}m^{-1}$
μ_0	Magnetic permeability	$4\pi.10^{-7}\ Hm^{-1}$
λ	Thermal conductivity of the billet	$206\ Wm^{-1}K^{-1}$
ρ	Specific mass of the billet	$2707\ kgm^{-3}$
c	Specific heat of the billet	$936\ Jkg^{-1}K^{-1}$

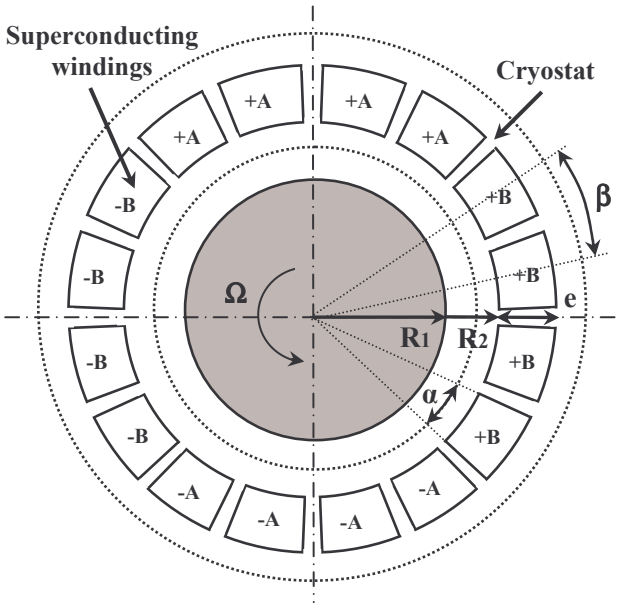

Fig. 1. Cross section of the 2 poles induction heater configuration.

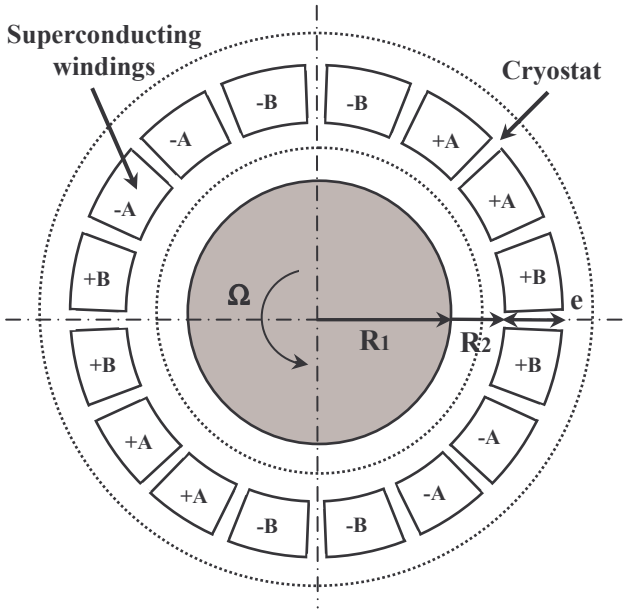

Fig. 2. Cross section of the 4 poles induction heater configuration.

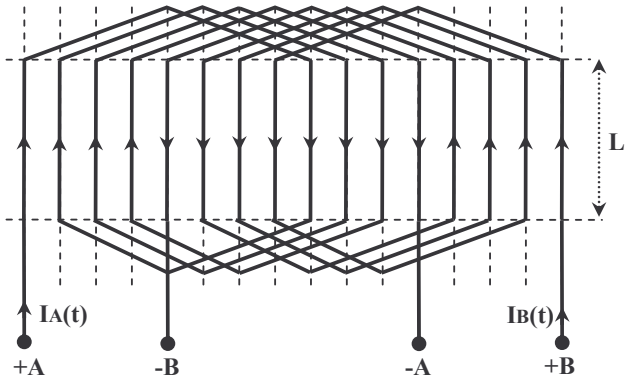

Fig. 3. 2 phase, 2 poles superconducting windings configuration.

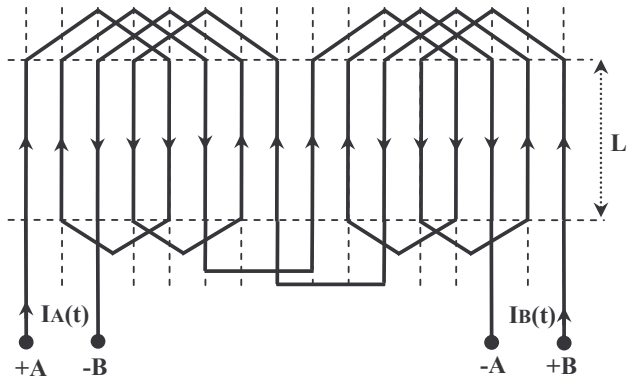

Fig. 4. 2 phase, 4 poles superconducting windings configuration.

III. Equivalent Current Sheet

The model of the induction heater used for analysis is shown in Fig. 5. We consider a solid conducting cylinder (aluminum billet) that has a radius R_1 and an infinite axial length. The cylinder can rotate around the z axis with a constant angular velocity Ω. For the analysis, it is assumed that the current flowing in the superconducting windings is replaced by a current sheet of radius $R_2 + e/2$ and infinite axial length [9]. This current sheet is chosen to carry exactly the same current as the original windings. For the analysis, only the fundamental component of the current sheet in space will be considered

$$K_z = K_{z1} \cdot cos(p\theta) \tag{1}$$

where K_{z1} is the peak value of the fundamental term of the current sheet in (A/m) and p is the number of poles pairs.

For engineering purpose, it is important to have a relation between the current density J flowing through the superconducting winding and the peak value of the current sheet K_{z1} defined in (1). The winding distribution (winding B) and its current sheet approximation for the 2 poles induction heater configuration are shown in Fig. 6. The winding B is excited with a DC current density J. The electrical current flowing through the winding B is given by

$$I_B = eJ\alpha \cdot \left(R_2 + \frac{e}{2} \right) \tag{2}$$

The corresponding value of the current sheet in A/m is then

$$K = eJ \tag{3}$$

The current sheet distribution versus circular angle θ is shown in Fig. 7. Its Fourier series expansion is

$$K_z(\theta) = \sum_{n=1}^{\infty} \frac{8eJ}{n\pi} sin\left(\frac{n\alpha}{2}\right)\left(cos\frac{n\beta}{2} + cos\frac{3n\beta}{2}\right) \cdot cos(n\theta) \tag{4}$$

By using only the fundamental term (n = 1) of the Fourier series expansion (4), we obtain a simple relation between J and K_{z1}

$$K_{z1} = \frac{8eJ}{\pi} \cdot sin\left(\frac{\alpha}{2}\right) \cdot \left(cos\frac{\beta}{2} + cos\frac{3\beta}{2}\right) \tag{5}$$

The magnetic flux lines distribution obtained for the winding B excited with a DC current density $J = 200$ A/mm^2 and the conducting cylinder at standstill is given in Fig. 8. The one obtained with the current sheet excitation with $K_{z1} = 5.79.10^6$ A/m (which is calculated using (5)) is given in Fig. 9. It can be observed that the magnetic flux line

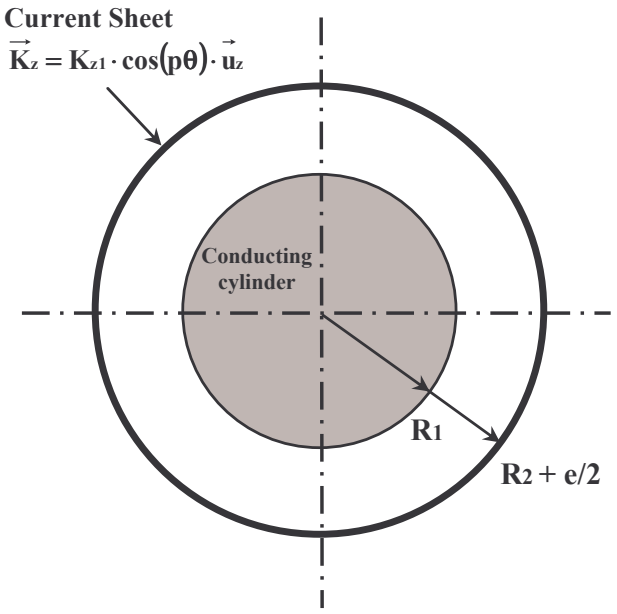

Fig. 5. First space harmonic current sheet approximation used for the analysis.

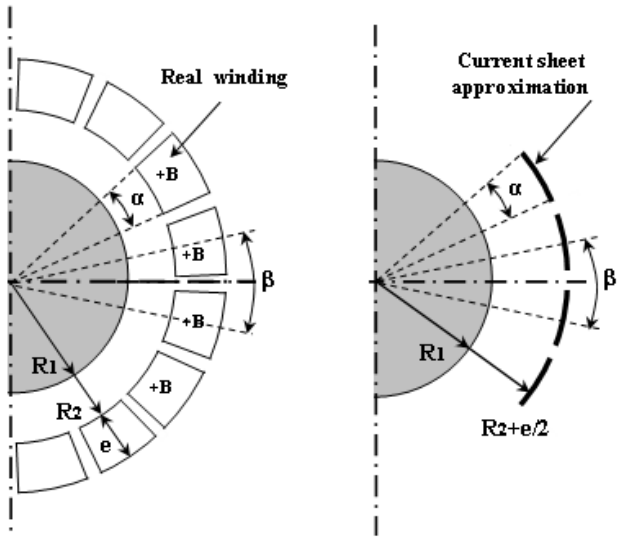

Fig. 6. Superconducting winding B configuration and its current sheet approximation.

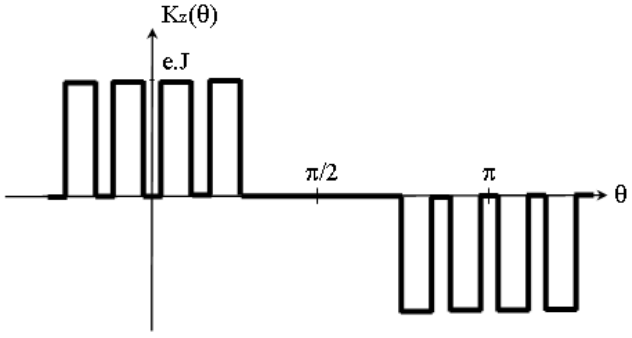

Fig. 7. Current sheet distribution versus circular angle θ.

distributions are almost the same in the region of the conducting cylinder. The corresponding magnetic flux density amplitudes at the circular lines $r = 5\,\text{cm}$ and $r = 8\,\text{cm}$ are shown in Fig. 10. As it is known, we can observe that the magnetic flux density generated by the 2 poles current sheet excitation is homogeneous inside the current sheet cylinder and its expression is

$$B = \frac{\mu_0 \cdot K_{z1}}{2} = 3.59\,\text{T} \tag{6}$$

On the other hand, the magnetic flux density generated by the winding B shows some variations around a mean value of about 3.5 T. The error introduced when using the fundamental term of an approximate current sheet excitation is relatively small especially for weak value of the *r* coordinate. For the circular line $r = 5\,\text{cm}$, the difference is inferior to 5%. As the cylinder to be heated must be distant from the superconducting winding for thermal insulation reasons, calculations that follow (eddy currents inside the cylinder) will be precise.

For the 4 poles induction heater configuration, the Fourier series expansion of the current sheet distribution and its fundamental term expression are

$$K_z(\theta) = \sum_{n=1}^{\infty} \frac{8eJ}{n\pi} sin(n\alpha) cos\, n\beta \cdot cos(2n\theta) \tag{7}$$

$$K_{z1} = \frac{8eJ}{\pi} \cdot sin(\alpha) \cdot cos(\beta) \tag{8}$$

With a DC current density $J = 200\,\text{A/mm}^2$, we obtain a value of $K_{z1} = 5.81.10^6$ A/m for the 4 poles configuration.

IV. Magnetic Field And Eddy Current Analysis

A general multiregion problem is analyzed. The whole space is divided into three regions as shown in Fig. 11. Region 1 corresponds to the conducting cylinder, region 2 to the space between the conducting cylinder and the current sheet and region 3 to the space outside the current sheet. As the configuration is circular, the cylindrical coordinate (*r, θ, z*) will be used. Because the conducting cylinder and the current sheet are considered infinitely long in the *z* direction, all magnetic quantities become independent of *z*. The problem is to determine the eddy currents in the cylinder and their corresponding power loss.

The magnetic problem is solved in the general case with rotating cylinder and sinusoidal excitation of the windings A and B. To obtain a rotating field, the windings must be fed by alternating currents with a phase shifted by 90 degrees. The equivalent current sheet expression is then

$$K_z = K_{z1} \cdot cos(p\theta - \omega t) \tag{9}$$

where ω is the electrical frequency of the AC current.

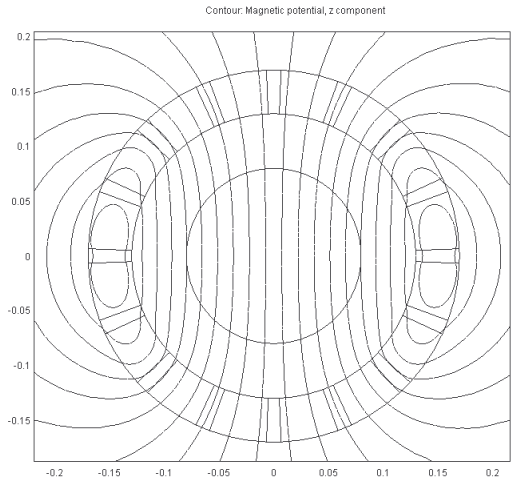

Fig. 8. Flux lines distribution for the 2 poles configuration and winding B fed by DC current (cylinder at standstill).

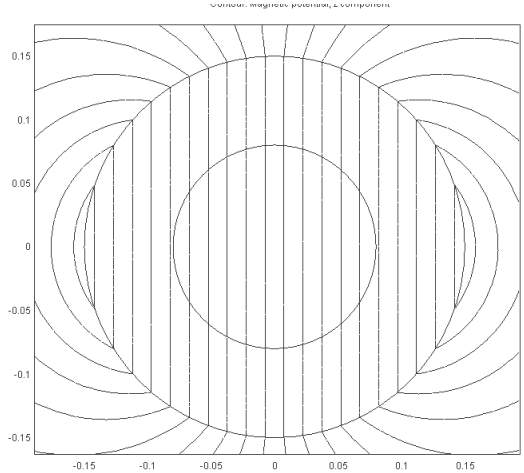

Fig. 9. Flux lines distribution for the 2 poles configuration with current sheet excitation (cylinder at standstill).

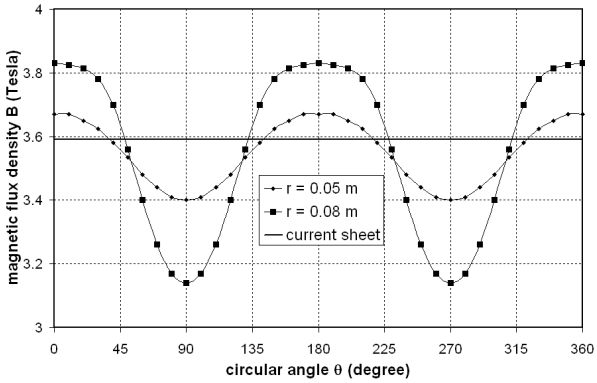

Fig. 10. Comparison between the magnetic flux density amplitude obtained with winding B fed by DC current and with current sheet excitation (cylinder at standstill).

A. Diffusion equation

The frequency of the source current is low, so the displacement current is assumed to be neglected and the Maxwell's equations are expressed as

$$\vec{\nabla}\times\vec{H}=\vec{J} \qquad \vec{\nabla}\times\vec{E}=-\frac{\partial\vec{B}}{\partial t} \qquad \vec{\nabla}\cdot\vec{B}=0 \qquad \vec{\nabla}\cdot\vec{E}=0 \tag{10}$$

This system of equations is coupled with relations associated to material properties

$$\vec{J}=\sigma\left(\vec{E}+\vec{v}\times\vec{B}\right) \quad \text{with} \quad \vec{v}=\Omega\cdot r\cdot\vec{u}_\theta \qquad \vec{\mathrm{B}}=\mu_0\cdot\vec{H} \tag{11}$$

The term $\vec{v}$ represents the linear velocity of the conductor material.

The magnetic vector potential is defined by

$$\vec{B}=\vec{\nabla}\times\vec{A} \quad \text{and} \quad \vec{E}=-\frac{\partial\vec{A}}{\partial t} \tag{12}$$

Using equations (10), (11) and (12), we obtain the magnetic diffusion equation which takes into account the movement of the cylinder

$$\nabla^2\vec{A}=\sigma\mu_0\cdot\left(\frac{\partial\vec{A}}{\partial t}-\vec{v}\times\vec{\nabla}\times\vec{A}\right) \tag{13}$$

The magnetic vector potential has an unique component in the z direction, then (13) becomes in 2-dimensional cylindrical coordinates

$$\frac{\partial^2 A}{\partial r^2}+\frac{1}{r}\frac{\partial A}{\partial r}+\frac{1}{r^2}\frac{\partial^2 A}{\partial\theta^2}=\sigma\mu_0\frac{\partial A}{\partial t}+\sigma\mu_0\Omega\frac{\partial A}{\partial\theta} \tag{14}$$

B. Magnetic vector potential expression

According to the form of the current sheet excitation (9), it is assumed that the solution of the magnetic vector potential in all space is given by [10]

$$A(r,\theta,t)=A(r)\cdot\cos\left(p\theta-\omega t+\varphi(r)\right) \tag{15}$$

Since the magnetic vector potential is varying sinusoidally in space and time, it is convenient to use the complex notation

$$A(r,\theta,t)=\Re\left\{\overline{A}e^{jp\theta}e^{-j\omega t}\right\} \text{ with } \overline{A}=A(r)\cdot e^{j\varphi(r)} \tag{16}$$

where $\Re$ denote the real part of the complex number. In the complex domain, (14) becomes a Bessel differential equation

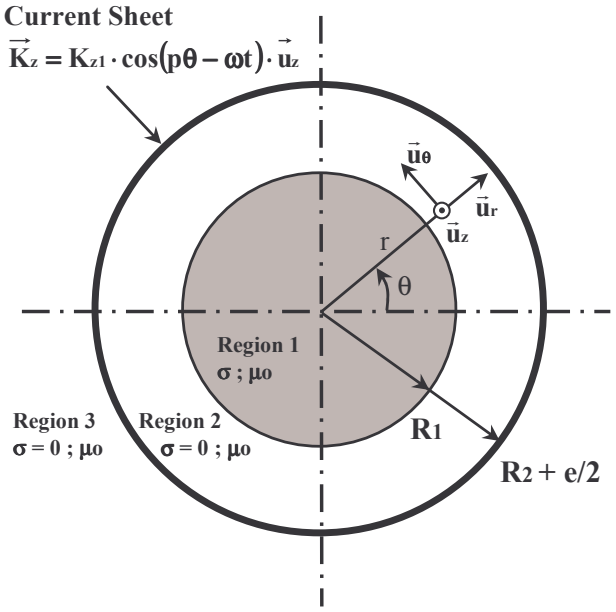

Fig. 11. Model of the induction heater used for the analysis.

$$r^2\frac{d\overline{A}}{dt}+r\frac{d\overline{A}}{dr}-\left(p^2+jk^2r^2\right)\cdot\overline{A}=0 \qquad \text{with} \quad k^2=\sigma\mu_0\cdot\left(p\Omega-\omega\right) \tag{17}$$

It can be seen in (17) that the electrical speed of the cylinder $p\Omega$ and the electrical frequency ω have the same effect on the value of k which is related to the classical skin depth δ by:

$$\delta=\frac{\sqrt{2}}{k} \tag{18}$$

By solving (17), we obtain a solution for each region. Magnetic vector potential in each region will be indicated by the suffixes 1, 2 and 3.

In the conducting cylinder (Region 1), the general solution of equation (17) can readily be determined by classical analytical methods [11] respecting that $\overline{A}_1$ must be finite when $r\to 0$

$$\overline{A}_1(r)=\alpha\cdot J_p\left(j^{\frac{3}{2}}kr\right) \quad \text{with} \quad j^2=-1 \tag{19}$$

where J_p is the Bessel function of the first kind and order p.

For region 2 where the electrical conductivity σ = 0, equation (17) becomes an Euler equation and the general solution is

$$\overline{A}_2(r)=\beta\cdot r^{-p}+\gamma\cdot r^{p} \tag{20}$$

For region 3, (17) is also an Euler equation. Knowing that $\overline{A}_3$ must be finite when $r \to \infty$, the solution is

$$\overline{A}_3(r) = \lambda \cdot r^{-p} \tag{21}$$

The constants α, β, γ and λ can be determined from the interface conditions between the different regions. The interface conditions are as follows

$$\overline{A}_1 = \overline{A}_2 \quad \text{and} \quad \frac{\partial \overline{A}_1}{\partial r} = \frac{\partial \overline{A}_2}{\partial r} \quad \text{for} \quad r = R_1 \tag{22}$$

$$\overline{A}_2 = \overline{A}_3 \quad \textit{and} \quad \frac{\partial \overline{A}_2}{\partial r} = \frac{\partial \overline{A}_3}{\partial r} + \mu_0 \cdot K_{z1} \quad \textit{for} \quad r = R_2 + \frac{e}{2} \tag{23}$$

Thus, we obtain a system of four linear equations which allow to determine the expressions of the constants α, β, γ and λ. The expression of the magnetic vector potential in region 1 is then

$$\overline{A}_1(r) = \frac{\mu_0 \cdot K_{z1} \cdot \left(R_2 + \frac{e}{2} \right)^{-p+1} \cdot {R_1}^{p-1}}{j^{\frac{3}{2}} \cdot k \cdot J_{p-1}\left(j^{\frac{3}{2}} k R_1 \right)} \cdot J_p\left(j^{\frac{3}{2}} k r \right) \tag{24}$$

Where J_{p-1} is the Bessel function of the first kind and order $(p - 1)$.

C. Eddy current expression

The induced current density in the cylinder can be obtained from the following equation

$$\vec{J}_1(r) = -\sigma \left(\frac{\partial \vec{A}_1}{\partial t} + \Omega \frac{\partial \vec{A}_1}{\partial \theta} \right) \tag{25}$$

which becomes in the complex domain

$$\overline{J}_1(r) = -j\sigma(p\Omega - \omega)\overline{A}_1 = -j\frac{k^2}{\mu_0}\overline{A}_1(r) \tag{26}$$

It finally gives the density of cylinder eddy current as

$$J_1(r,\theta,t) = \Re\left\{ \overline{J}_1(r) \cdot e^{jp\theta} e^{-j\omega t} \right\} \tag{27}$$

D. Eddy-current power loss expression

The eddy current power loss density is given by

$$p(r,\theta,t) = \frac{{J_1}^2(r,\theta,t)}{\sigma} \tag{28}$$

The average eddy-current power loss in the cylinder can be evaluated by integrating the power loss density over the volume of the cylinder

$$P = \frac{L}{T} \int_T \left\{ \int_0^{R_1} \int_0^{2\pi} \frac{{J_1}^2(r,\theta,t)}{\sigma} r dr d\theta \right\} dt \tag{29}$$

where L is the axial length of the cylinder.

Substituting (24) and (26) into (27) and then (27) into (29), we obtain the following analytical expression for the average power loss in the cylinder for a *2p* poles configuration

$$P_p = \frac{L \cdot \pi \cdot k^2 \cdot {K_{z1}}^2 \cdot \left(\left(R_2 + \frac{e}{2} \right)^{-p+1} \cdot {R_1}^{p-1} \right)^2}{\sigma \cdot J_{p-1}\left(j^{\frac{3}{2}} k R_1 \right) \cdot J_{p-1}\left(j^{-\frac{3}{2}} k R_1 \right)} \cdot M \tag{30}$$

With

$$M = \frac{R_1}{2k} \cdot \left\{ j^{-\frac{1}{2}} \cdot J_p\left(j^{\frac{3}{2}} k R_1 \right) \cdot J_{p-1}\left(j^{-\frac{3}{2}} k R_1 \right) + j^{\frac{1}{2}} \cdot J_p\left(j^{-\frac{3}{2}} k R_1 \right) \cdot J_{p-1}\left(j^{\frac{3}{2}} k R_1 \right) \right\}$$

Expression (30) can be simplified in the case of low difference between electrical frequency ω and angular electrical speed $p\Omega$ when [11]

$$k \cdot R_1 < 1 \tag{31}$$

With this assumption, the impact of eddy-currents magnetic field on themselves is neglected. Using limited series expansion of Bessel functions, one can find a simplified expression of (30). In the case of 2 and 4 poles configuration, we obtain

$$P_1 = \frac{1}{16} L\pi\sigma \cdot \left(\mu_0 K_{z1} \right)^2 \cdot (\Omega - \omega)^2 \cdot {R_1}^4 \tag{32}$$

$$P_2 = \frac{1}{96 \cdot \left(R_2 + \frac{e}{2} \right)^2} L\pi\sigma \cdot \left(\mu_0 K_{z1} \right)^2 \cdot (2\Omega - \omega)^2 \cdot {R_1}^6 \tag{33}$$

The average power losses are then a quadratic function of the frequency. These analytical expressions can be used as a tool for design optimization of the induction heater.

V. Results Verification

A. Eddy current density

The results are given for the conducting cylinder rotating in a DC magnetic field (ω=0). This operating mode is more interesting for superconducting coils which present no loss when they are fed by DC current (this is not the case with AC current). However, this operating mode is technically more complicated.

Fig. 12 and Fig. 13 show the magnetic flux lines distribution obtained with FEM when the winding B is fed by a DC current density $J = 200\ \mathrm{A/mm^2}$ and the conducting cylinder rotating respectively at an angular speed of $\Omega = 3\ \mathrm{rad/s}$ and $\Omega = 30\ \mathrm{rad/s}$. The corresponding eddy current density distributions inside the cylinder are given in Fig. 14 and Fig. 15. We can observe that the results obtained with the analytical method (current sheet method) match well with those obtained by FEM (with real winding distribution).

The contour plots of the magnetic flux amplitude for the 4 poles configuration and the corresponding eddy current distributions are given from Fig. 16 to Fig. 19.

B. Eddy current losses

Table II gives the values of the average power losses in the cylinder for the two operating modes (rotating cylinder and rotating field) in the same conditions of current density amplitude and frequency. These results have been obtained with the analytical expression (30) and with the FEM (Comsol). One can observe that approximately the same results are obtained for the two operating modes with the same values of the current density (amplitude) in the windings and with the same frequency/speed. These results confirm that

TABLE II
COMPARISON BETWEEN AVERAGE POWER LOSSES (KW) FOR THE TWO OPERATING MODE

	Analytical results (30)		FEM (real windings)	
	p=1	p=2	p=1	p=2
Rotating cylinder Ω =3 rad/s; J_{DC} = 200 A/mm^2	201.3	38.9	191.8	39.6
Rotating field $\omega = p\Omega$; J_{AC} = 200 A/mm^2	201.3	38.9	190.9	39.6

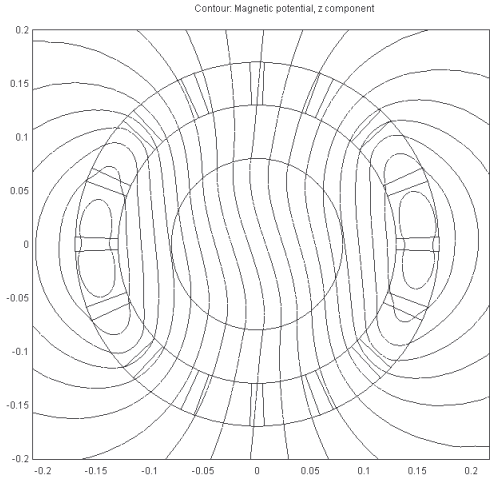

Fig. 12. Flux lines distribution for the 2 poles configuration with Ω = 3 rad/s.

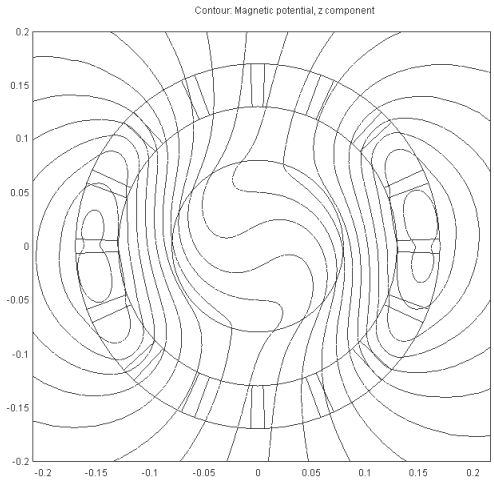

Fig. 13. Flux lines distribution for the 2 poles configuration with Ω = 30 rad/s.

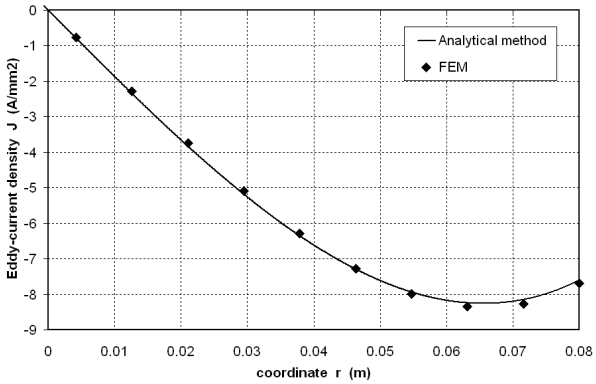

Fig. 14. Eddy current density in terms of the radial distance r (at $\theta = 0°$) for the 2 poles configuration with Ω = 3 rad/s.

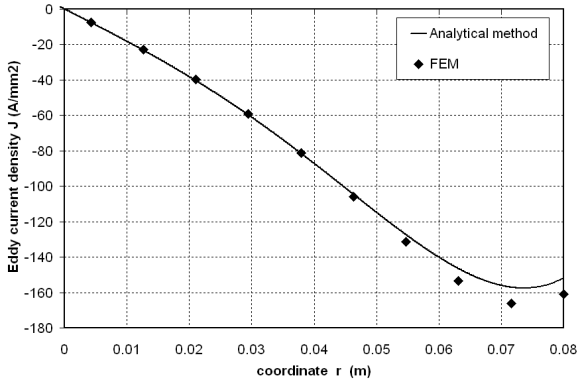

Fig. 15. Eddy current density in terms of the radial distance r (at $\theta = 0°$) for the 2 poles configuration with Ω = 30 rad/s.

taking approximately the first space harmonic for the current distribution is a good approximation for the analysis of the two operating modes.

The average power loss in the cylinder obtained for various values of the rotation speed Ω and for the winding B excited by a DC current density $J = 200\ \text{A/mm}^2$ is given in Fig. 20. The analytical results derived with the complete expression of the power loss (30) and with the approximate expressions (32) and (33) are compared with the ones obtained from the FEM. It can be shown that the analytical results correspond closely to the one obtained with FEM. We can see in Fig. 20 that the approximate expression for the power loss (p = 1) is of acceptable accuracy for $\Omega \leq 3\ \text{rad/s}$, the margin of error is about 5%. One can also observe that the power loss in the cylinder are more important for the 2 poles configuration (p = 1) than for the 4 poles configuration (p = 2) for the same condition of the current density in the superconducting winding.

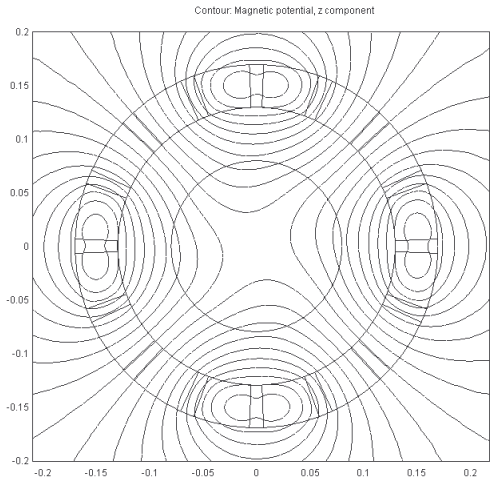

Fig. 16. Flux lines distribution for the 4 poles configuration with Ω = 3 rad/s

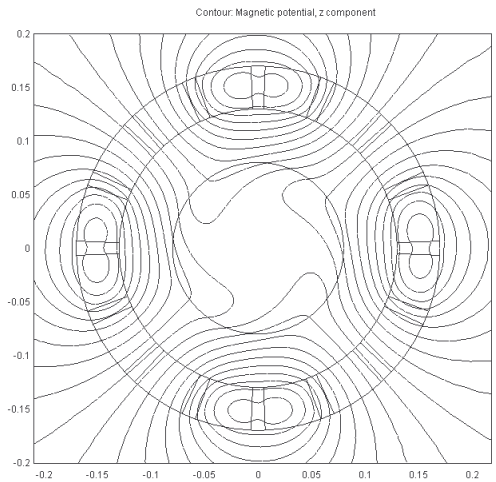

Fig. 17. Flux lines distribution for the 4 poles configuration with Ω = 30 rad/s.

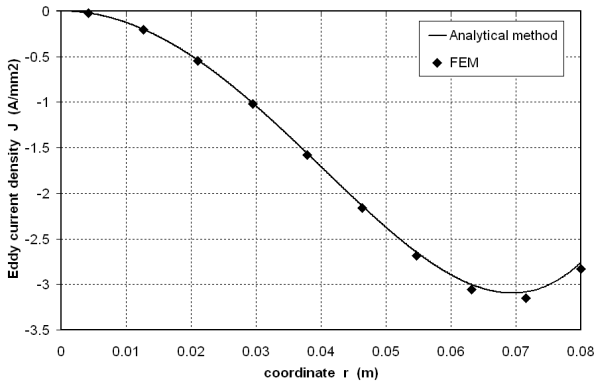

Fig. 18. Eddy current density in terms of the radial distance r (at $\theta = 0°$) for the 4 poles configuration with Ω = 3 rad/s.

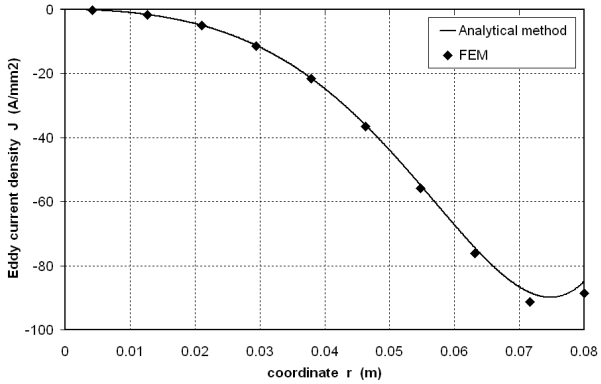

Fig. 19. Eddy current density in terms of the radial distance r (at $\theta = 0°$) for the 4 poles configuration with Ω = 30 rad/s.

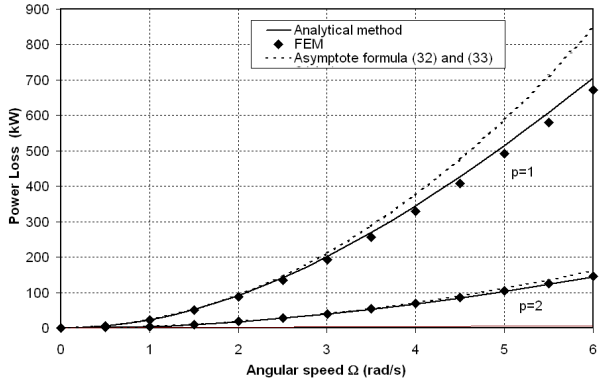

Fig. 20. Power loss versus angular speed Ω for $J = 200\ \text{A/mm}^2$.

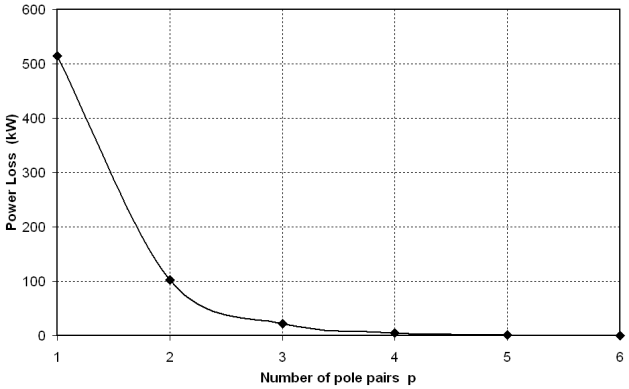

Fig. 21. Effect of the number of pole pairs on the power loss for Ω = 5 rad/s.

C. Influence of the number of pole pairs

Fig. 21, obtained with the analytical formula (30), shows the influence of the number of pole pairs on the eddy-current power loss for $\Omega = 5$ rad/s and $J = 200$ A/mm^2. The eddy-current power loss decreases very rapidly with the number of pole pairs. The 2 poles induction heater configuration is the best one in terms of heat power transfer.

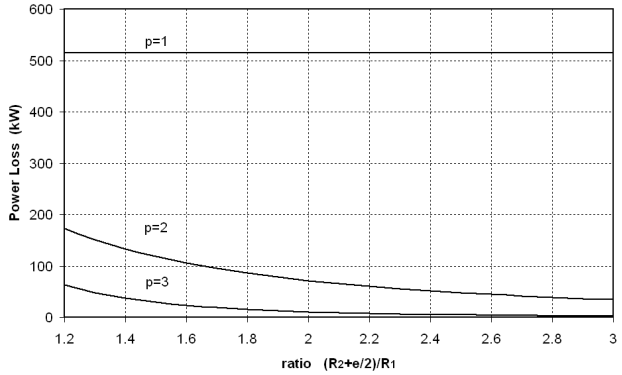

Fig. 22. Effect of the ratio $(R_2+e/2)/R_1$ on the eddy-current power loss for $\Omega = 5$ rad/s, $J = 200$ A/mm^2 and $R_1 = 8$ cm.

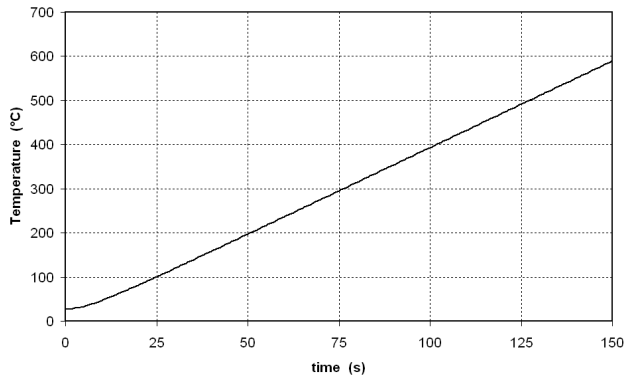

Fig. 23. Transient temperature profile at the center of the cylinder for $\Omega = 3$ rad/s and $J = 200$ A/mm^2

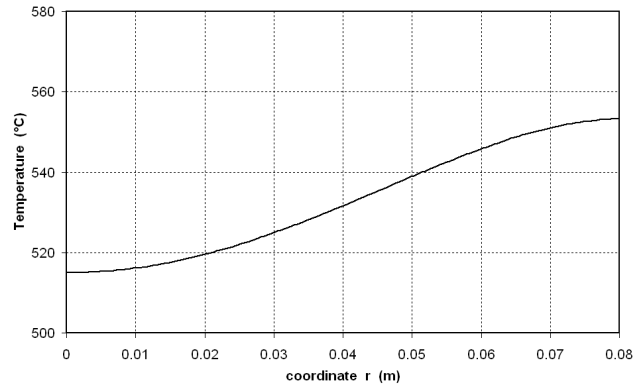

Fig. 24. Temperature distribution in the cylinder in terms of the radial distance r for : $\Omega = 3$ rad/s and $J = 200$ A/mm^2.

D. Influence of the distance between the superconducting windings and the conducting cylinder

It is also interesting to study the influence of the ratio $(R_2+e/2)/R_1$ on the eddy-current power loss (the other parameters are maintained constant) to show the influence of the distance between the superconducting windings and the conducting cylinder. A certain distance is necessary to place the superconducting windings inside the cryostat and to place a thermal insulation between the cylinder to be heated and the cryostat. It can be shown in (30) and in Fig. 22 (obtained with analytical formula) that the power losses are independent of $(R_2+e/2)$ for the 2 poles induction heater configuration ($p = 1$). In this particular case, it is known that the flux density developed by the current sheet is independent of $(R_2+e/2)$ and therefore the average power losses too. For a number of pole pairs greater than 1, the eddy-current power loss decreases when the distance between the superconducting winding and the conducting cylinder increases.

VI. Temperature Field Analysis

The temperature field inside the cylinder can be described in a stationary co-ordinate system by the transient heat transfer equation which takes into account the movement of the cylinder

$$\rho c\left(\frac{\partial T}{\partial t}+\vec{v}\cdot\vec{\nabla}T\right)=p(r,\theta,t)+\lambda\Delta T \tag{34}$$

where T is the temperature, λ is the thermal conductivity of the cylinder, ρ its specific mass and c its specific heat. The values of λ, ρ and c are given in Table I.

The term $\vec{v}\cdot\vec{\nabla}T$ in (34) is due to the movement of the cylinder [13]. The heat source distribution $p(r,\theta,t)$ produces by eddy-current in the cylinder is given in (28). The temperature field is solved only in the region of the conducting cylinder (region 1). In 2-dimensional cylindrical coordinates, the thermal problem assuming adiabatic boundary condition at the surface of the cylinder and constant initial condition is written as

$$\rho c\left(\frac{\partial T}{\partial t}-\Omega\frac{\partial T}{\partial \theta}\right)=p(r,\theta,t)+\lambda\left(\frac{\partial^2 T}{\partial r^2}+\frac{1}{r}\frac{\partial T}{\partial r}+\frac{1}{r^2}\frac{\partial^2 T}{\partial \theta^2}\right) \tag{35a}$$

$$-\lambda\left.\frac{\partial T}{\partial r}\right|_{r=R_1}=0 \tag{35b}$$

$$T(r,\theta,t=0)=30°C \tag{35c}$$

The thermal problem was solved with two-dimensional finite element method software (COMSOL). The study has been made only for constant velocity of the cylinder. The eddy-current power loss density is calculated in a first step

and the result is stored as the source terms to be used in the heat equation (35a).

Fig. 23 shows the transient temperature profile at the center of the cylinder. The angular speed of the cylinder is fixed at $\Omega = 3$ rad/s and the current density in the superconducting winding is fixed at $J = 200$ A/mm^2. Theses values correspond to an average power loss of 200 kW in the cylinder. Because of the adiabatic boundary condition, the temperature rise inside the cylinder is almost linear. The rise time to heat the cylinder from 30 °C to 500 °C is about two minutes.

Fig. 24 shows the temperature distribution inside the cylinder in terms of the radial distance r at time t = 130s. The results obtained with the FEM have shown that the temperature distribution in the cylinder does not depend of the θ coordinate. The maximum temperature is T = 555 °C on the surface of the cylinder and the minimum temperature is T = 515 °C at the center of the cylinder, which correspond to a variation of ± 3.7% around the mean value. In that case, the temperature distribution is sufficiently homogeneous inside the cylinder for press-forming operation (the temperature uniformity must be within ± 5%).

The value of the ratio R_1/δ (where δ is the skin depth defined in (18)) affects the temperature distribution inside the cylinder. The result shown in Fig. 24 corresponds to a ratio R_1/δ = 0.8 ($\Omega = 3$ rad/s). In order to study the influence of R_1/δ on the temperature distribution, we compare, in Fig. 25, the results obtained for $\Omega = 3$ rad/s and for $\Omega = 314$ rad/s, which correspond respectively to R_1/δ = 0.8 and R_1/δ = 8.3. The current density in the winding has been chosen to obtain the same average losses in the cylinder (200 kW) for the two cases ($J = 200$ A/mm^2 for $\Omega = 3$ rad/s and $J = 23.1$ A/mm^2 for $\Omega = 314$ rad/s). We can observe that the temperature variation is more important when R_1/δ = 8.3. In that case, the temperature uniformity is only equal to ± 6.7%. Fig. 26 gives the variation of the temperature uniformity as a function of R_1/δ. As the temperature uniformity must be within ± 5% to avoid cracking or local melting during the press forming operation, the value of R_1/δ must satisfy the condition

$$\frac{R_1}{\delta} \leq 3 \tag{36}$$

For R_1 = 8 cm, this expression corresponds to a maximum speed of $\Omega = 40$ rad/s. The choice of the rotating speed (or electrical frequency) depends of the desired average power loss in the cylinder. For an average power of 200 kW (with $J = 200$ A/mm^2), we must choose $\Omega = 3$ rad/s (R_1/δ = 0.8).

It is important to keep in mind that the analysis developed in the paper is a simplification of a 3D problem to a 2-dimensional one. Indeed, we have supposed an infinitely long cylinder whereas the length of the cylinder is finite. The study developed in [14] which takes into account the 3D effects has shown that the heads of the cylinder is colder than the center. This is due to the fact that the power density induced in the end regions is smaller than in the lateral surface of the cylinder. However, we suppose that the use of low frequency for the induction heater will allow a relatively good homogeneity temperature along the cylinder. We will verify this hypothesis in future work with the development of a 3D numerical study of the problem

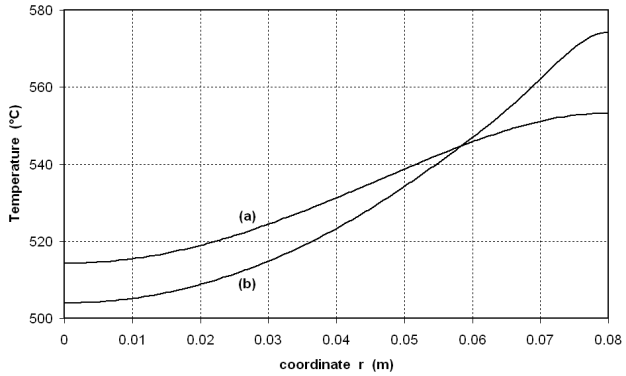

Fig. 25. Temperature distribution in the cylinder in terms of the radial distance r for: (a) Ω = 3 rad/s and R_1/δ = 0.8; (b) Ω = 314 rad/s and R_1/δ = 8.3.

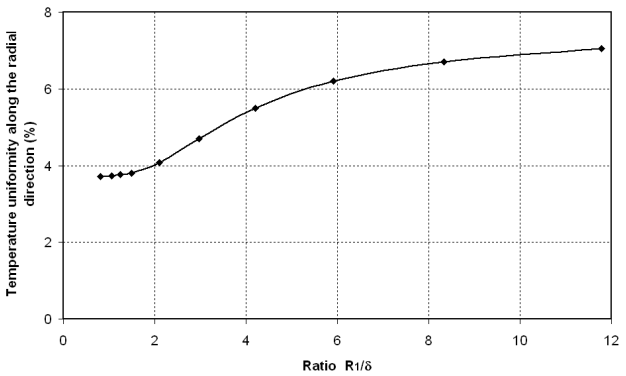

Fig. 26. Temperature uniformity along the radial direction of the cylinder versus (R_1/δ).

VII. Conclusion

We have presented in this paper an original structure of induction heater for aluminum billets using superconducting windings. With the proposed structure, the billet to be heated is subjected to a high magnitude rotating magnetic field of low frequency. The rotating magnetic field seen by the billet can be obtained by two different ways with the same geometrical structure of the induction heater. Either the billet rotates at constant velocity in magnetic field due to a DC current or the billet is at rest and subjected to a rotating magnetic field produced by two phase superconducting windings. An analytical solution of eddy-current power loss has been developed for a 2p poles configuration and has been validated using a FEM software. The study has shown that the 2 poles configuration is the best one in terms of heat power transfer. The 2 poles configuration is also suitable because the heat power transfer is independent of the distance between the

billet and the superconducting windings what allows to place the cryostat far from the billet. We also shown that with the use of strong magnetic field of low frequencies (rotating speed or AC current pulsation), the heat power is induced in the heart of the billet and allows to obtain a homogeneous temperature which is good for press-forming of aluminum billet

REFERENCES

[1] V. Rudnev, D. Loveless, R. Cook and M. Black, *Handbook of induction heating,* Marcel Dekker inc., New York, 2003..

[2] M. Runde and N. Magnusson, "Induction heating of aluminum billets using superconducting coils*," Physica C*, vol. 372-376, pp. 1339-1341, Aug. 2002.

[3] M. Runde and N. Magnusson, "Design, building and testing of a 10 kW superconducting induction heater*," IEEE Trans. Appl. Supercond.,* vol. 13, no. 2, pp. 1612-1615, Jun. 2003

[4] N. Magnusson and M. Runde, "Efficiency analysis of a high-temperature superconducting induction heater*," IEEE Trans. Appl. Supercond.,* vol. 13, no. 2, pp. 1616-1619, Jun. 2003

[5] N. Magnusson and M. Runde, "A 200 kW MgB2 induction heater project*," J. Phys.: Conf. Ser.*, vol. 43, pp. 1019-1022, 2006.

[6] A. Stenvall et al., "Electromagnetic viewpoints on a 200 kW MgB2 induction heater*," Physica C*, vol. 463, no. 6, pp. 487-491, May. 2008.

[7] I. Hiltunen et al. "Cryogenic design of the Aluheat project*," Trans. Cryogenic Engineering Conf.*, vol. 985, pp. 1015-1022, 2007.

[8] M. Fabbri, A. Morandi and F. Negrini, "Temperature distribution in aluminum billets heated by rotation in a static magnetic field produced by superconducting magnets*", COMPEL.,* vol. 24, no. 1, pp. 281-290, 2005

[9] L. M. Witkowski, P. Marty and J. S. Walker, "Multidomain analytical-numerical solution for rotating magnetic field with finite-length conducting cylinder*," IEEE Trans. Magn.,* vol. 36, no. 2, pp. 452-460, Mar. 2000.

[10] M. Markovic and Y. Perriard, "An analytical determination of eddy-current losses in a configuration with a rotating permanent magnet*," IEEE Trans. Magn.,* vol. 43, no. 8, pp. 3380-3386, Aug. 2007.

[11] M. Abramowitz and I. Stegun, *Handbook of mathematical function. New York: Dover, 1972*

[12] M. Perry and T. Jones, "Eddy current induction in a solid conducting cylinder with a transverse magnetic field*," IEEE Trans. Magn.,* vol. MAG-14, no. 4, pp. 227-232, Jul. 1978.

[13] Z. Wang, X. Yang, Y. Wang and W. Yan, "Eddy current and temperature field computation in transverse flux induction heating equipment for galvanizing line*" IEEE Trans. Magn.,* vol. 37, no. 5, pp. 3437-3439, Sep. 2001

[14] A. Morandi, M. Fabbri, and P.L. Ribani, "Design of a superconducting saddle magnet for dc induction heating of aluminum billets*," IEEE Trans. Appl. Supercond.,* vol. 18, no. 2, pp. 816-819, Jun. 2008

Manuscript received July 8, 2008. Corresponding author: Thierry Lubin (e-mail: thierry.lubin@green.uhp-nancy.fr).

Thierry Lubin was born in Sedan, France, in 1970. He received the M.S. Degree from the University of Paris 6, France in 1994 and the Ph.D. degree from the University Henri Poincaré, Nancy, France, in 2003.

He is currently a lecturer of Electrical Engineering at the University of Nancy at the Groupe de Recherche en Electrotechnique et Electronique de Nancy. His interests include modeling and control of electrical machine and applied superconductivity in electrical devices.

Denis Netter was born in Auchel, France, in 1969. He received the Ph. D. degree in electrical engineering from the Université Henri Poincaré, Nancy, France, in 1997.

He has been a lecturer of Electrical Engineering at the University of Nancy at the Groupe de Recherche en Electrotechnique et Electronique de Nancy since 1998. His research interests include superconducting devices (SMES, superconducting motors, loss calculation in high-temperature superconductors) and Monte Carlo methods applied to numerical solutions of Maxwell equations.

Jean Leveque was born in Angers, France, in 1963. He received the B.S. and M.S. degrees from the University of Nantes, France, in 1987 and 1988 and the Ph.D. degree from the Institut National Polytechnique de Grenoble, France, in 1993.

He joined the Groupe de Recherche en Electrotechnique et Electronique de Nancy, Université Henri Poincaré, Nancy, France, in 1993. He is currently a Professor at the University of Nancy, France. His current research concerns applied superconductivity. He works on superconducting current limiting devices, SMES, thermal processes in superconducting coil, and losses in superconducting wire.

Abderrezak Rezzoug received the Doctorat d'Etat from the Institut Nationale Polytechnique de Lorraine, France, in 1987.

After working at the INPL as an assistant Professor until 1991, he joined the Université Henri Poincaré, Nancy, France, as a Professor. He is currently the Dean of the laboratory Groupe de Recherche en Electrotechnique et Electronique de Nancy. His interests are in superconducting applications to electrical devices, and the control and diagnosis of electrical machines.